ELSEVIER

*Polymer* Vol. 37 No. 4, pp. 615–623, 1996

0032-3861/96/$15.00+0.00

# Effect of a plastic deformation on the nanostructure of polycarbonate: study by low-frequency Raman scattering

**A Mermet* and E. Duval**
*Laboratoire de Physico-Chimie des Matériaux Luminescents URA CNRS 442, Université Claude Bernard, 43 boulevard du 11 Novembre 1918, 69622 Villeurbanne Cedex, France*

**and S. Etienne and C. G'Sell**
*Laboratoire de Métallurgie Physique et Science des Matériaux URA CNRS 155, Ecole des Mines, Parc de Saurupt, 54042 Nancy, France*
*(Received 13 April 1995)*

The effect of a plastic deformation, induced by a simple shear, on the nanostructure of amorphous polycarbonate (PC), is studied by low-frequency Raman scattering (LFRS). As previously observed for poly(methyl methacrylate) (PMMA), an excess appears in the low-frequency part of LFRS spectra after plastic deformation. The excess is stronger in the case of PC than in the case of PMMA, and its light polarization, relative to the molecular orientation, is different. In the frame of a non-continuous glassy polymer network, the experimental results are interpreted by an orientation of macromolecular strands in the less cohesive zones of the polymer matrix, between the more cohesive regions. When the deformation is carried out at a temperature lower than the glass transition temperature, the more cohesive regions are not affected by the plastic deformation. It is no more the case when the polymer is deformed at a temperature higher than $T_g$.

**(Keywords: polycarbonate; plasticity; microstructure)**

## INTRODUCTION

Since the vibrational dynamics specifically depend on the bonding or cohesion in solids, they provide information about the structure. However, in spite of the many universal features that exhibit the dynamics of most glasses in the energy range 1–15 meV, the structure of amorphous materials is still a controversial topic. In the past decade, the Raman scattering technique has proved to be a powerful tool to investigate such a spectral range, extending from 2 up to 200 $cm^{-1}$ in wave numbers. The "universal" feature of glasses appears on low-frequency Raman scattering (LFRS) spectra as a peak located between 10 and 20 $cm^{-1}$ for amorphous polymers, called the "boson peak"[1–3]. It is now well established that the existence of the boson peak is related to the anomalous frequency dependence of the vibrational density of states (VDOS) of glasses. Such a relation is expressed by equation (1) which gives the LFRS intensity $I(\omega)$, for Stokes scattering[1–3]:

$$I(\omega) = C(\omega)g(\omega)\frac{n(\omega)+1}{\omega} \qquad (1)$$

where $C(\omega)$ is the light–vibration coupling coefficient; $g(\omega)$ the VDOS; and $n(\omega)$ the Bose factor.

* To whom correspondence should be addressed

Therefore, from equation (1), one can conclude that the LFRS yields a distorted picture of the VDOS because of its dependence on the coupling coefficient $C(\omega)$. However, several authors[4–7] found that $C(\omega)$ is proportional to $\omega$ in the frequency range 10–100 $cm^{-1}$, i.e., in the boson peak region, for amorphous polymers. Under such considerations, the VDOS is directly described by the reduced intensity:

$$I_R(\omega) = \frac{I(\omega)}{n(\omega)+1} \propto g(\omega) \qquad (2)$$

An interpretation for the non-Debye behavior of $g(\omega)$ ($g_{Debye} \propto \omega^2$) lies in the description of the glass as a non-homogeneous medium at the scale of a few nanometres. The glassy structure consists of highly cohesive regions separated from each other by comparatively less cohesive channels[8,9]. Such a cohesion contrast, although it is expected to be weak and hence most acutely felt by vibrations, gives rise to surface vibrational modes of the strongly bonded entities. According to this model, the frequency position of the boson peak is inversely proportional to the mean size of the nano-heterogeneities, which is about 4–5 nm in amorphous polymers[10].

On the basis of such a non-continuous glassy structure, effects of both a plastic deformation and thermal treatments were studied in PMMA[11]. In continuation of this work, we report here the results of

a similar investigation carried out on polycarbonate (PC). In the following section, a description of the PC samples deformed in different conditions is given. Then the LFRS technique is briefly described. The experimental results are presented in the next section and a detailed analysis of these is given in the discussion.

## SAMPLES AND MECHANICAL TESTING DEVICES

A commercial grade of polycarbonate was purchased from Bayer, whose number average molecular weight is about 15 600 g mol$^{-1}$ with a polydispersity index of 1.85. The glass transition temperature of this polymer is around 145°C, as determined by d.s.c.

The samples were machined from the extruded plates with a shape depicted in *Figure 1a*. The dimension of the calibrated part was $5 \times 4 \times 70\,mm^3$. Both planar and planar-concave calibrated parts were studied. From their initial shape (*Figure 1a*), the specimens were plastically deformed[12,13] in simple shear. Using a servo-hydraulic testing machine (MTS model 810), the local shear strain $\gamma(t)$ was monitored by means of a video camera which allows measurement of $\gamma$ through the inclination $\theta$ of a printed serigraphic ink marker on the calibrated part of the sample ($\gamma = \tan\theta$)[12,13]. A constant shear rate of $\dot{\gamma} = 5 \times 10^{-4}$ s$^{-1}$ was chosen in order to avoid any adiabatic heating during the deformation process. The shear stress $\tau(t)$ was recorded as the load per unit cross-section.

Four series of samples were studied, according to different types of shear strain pathways (*Figure 2*):

(1) undeformed specimens;
(2) specimens that were plastically deformed up to a shear strain $\gamma = 100\%$ (path ABCD). These are called 'deformed specimens';
(3) specimens that were first deformed up to $\gamma = 100\%$ and then sheared in the opposite direction until they were brought back to their initial shape, i.e., with a shear stress $\tau$ and a macroscopic strain $\gamma$ both equal to zero (path ABCDEFG). These are called 'cycled specimens';
(4) specimens that were first cycled and then sheared a second time in the direct sense, up to $\gamma = 90\%$ again (path ABCDEFGHI). These are called 'redeformed specimens'.

For these four series the tests were performed at room temperature, PC being capable of undergoing extensive plastic deformation well below $T_g$ without any damage.

Some PC specimens were deformed in simple shear around $T_g$, using the same experimental technique with the same parameters.

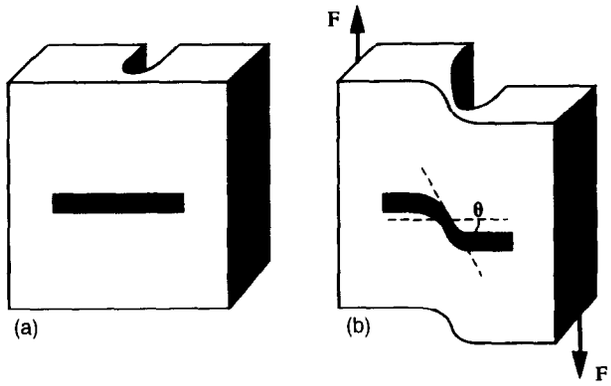


**Figure 1** Planar–concave calibrated part specimen geometry for simple shear test (a) before and (b) after deformation

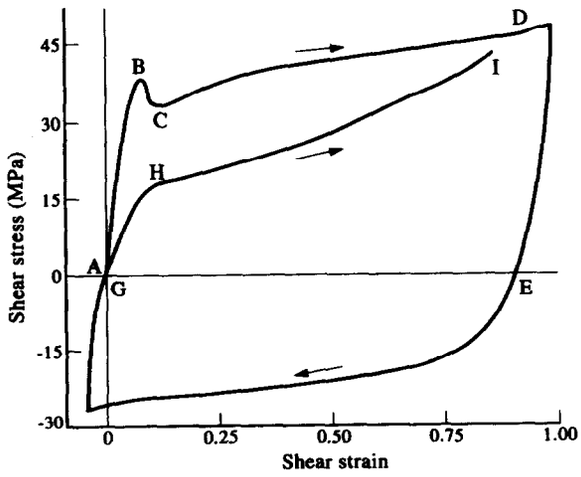


**Figure 2** Shear stress–strain pattern of PC at room temperature

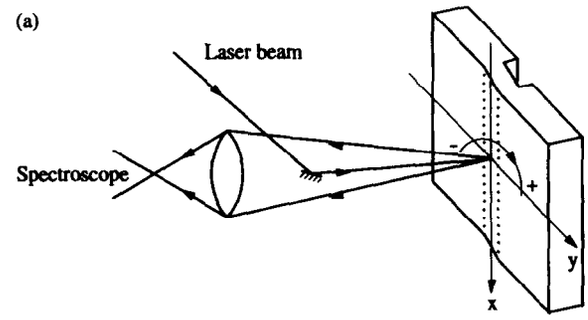


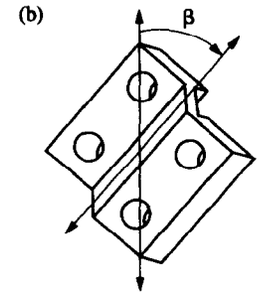


**Figure 3** (a) Optical arrangment for the Raman backscattering experiment (shown with a planar calibrated part specimen). (b) By rotating the sample around the laser beam direction, the dependence of the LFRS intensity on the relative direction of the incident light polarization with respect to that of the shear stress (angle β) could be studied

## RAMAN SCATTERING MEASUREMENTS

In order to avoid the fluorescence which screens the Raman signal when short-wavelength laser excitations are used, the 676.4 nm line of a Krypton laser was chosen. LFRS spectra were made with a high-resolution spectrometer (five additive monochromators) equipped with a photon counting system.

In order to probe the deformed part of the samples, a backscattering setup was chosen (*Figure 3*). By rotating the sample around the laser beam direction, the dependence on the angle $\beta$ between the incident light polarization and the shear stress direction could be studied. This angle $\beta$ was set positive for a rotation vector in the same direction as the shear torque momentum and the laser beam as shown in *Figure 3*.

By adjusting the polarization of the laser beam, both polarized (vertical incident light polarization and vertical analysed scattered light polarization, VV configuration) and depolarized (HV configuration) LFRS spectra could be recorded.

## RESULTS

Since a shear plastic deformation induces various changes in LFRS according to the corresponding plastic strain history, all spectra will be compared to that of the non-deformed sample thus taken as reference.

### *Undeformed samples*

Polarized LFRS direct ($I(\omega)$) and reduced ($I_R(\omega)$) intensities are displayed in *Figure 4*. The direct room temperature spectrum exhibits a monotonic behavior, while those taken at 200 K and 120 K exhibit a boson peak around 14 $cm^{-1}$. This peak merges into the quasielastic scattering for temperatures above 200 K.

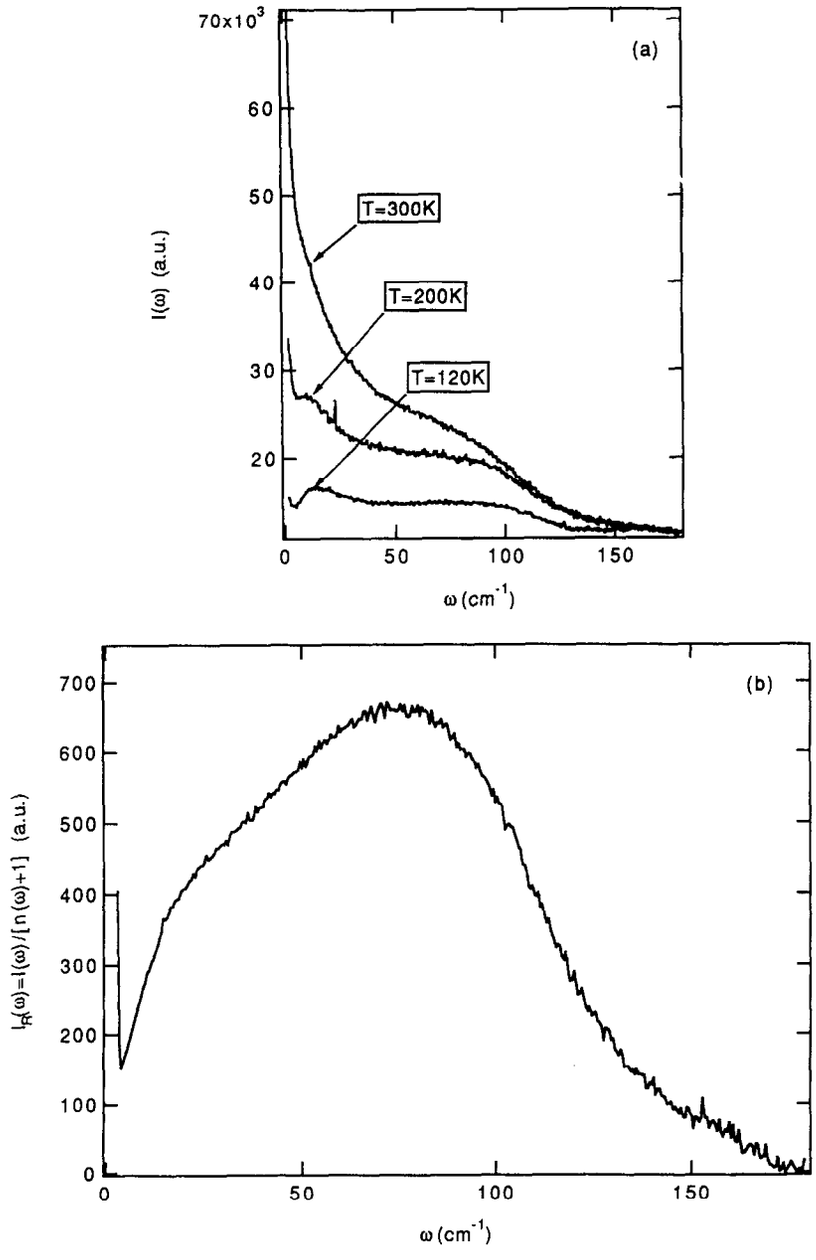


**Figure 4** LFRS (a) direct intensity $I(\omega)$ at three different temperatures and (b) reduced intensity $I_R(\omega)$ of undeformed PC at room temperature

The reduced intensity appears as a broad band, with a maximum around $80\,cm^{-1}$: it is ascribed to scattering by acoustic vibrational modes which are non-propagative ($k \approx 0$) because of the structural disorder. A shoulder is observed on the left wing of the broad band: it is reminiscent of the boson peak which sharply appears on low-temperature $I(\omega)$ spectra. As both the room and low-temperature reduced intensities $I_R(\omega)$ lead to the same kind of information, the Raman scattering experiments were all conducted at 300 K, on grounds of simplicity.

As expected, these spectra are dependent on the β angle values, thus confirming the isotropy of non-deformed PC.

*Deformed samples*

The room temperature reduced polarized intensity $I_R(\omega)$ of the deformed and the non-deformed samples ($\beta = 0°$) are shown in *Figure 5a*. In order to make reliable comparisons, all reduced spectra were normalized with respect to the broad band maximum around $80\,cm^{-1}$.

As previously observed with PMMA samples[11], an increase of scattering appears from $4\,cm^{-1}$ up to the broad band maximum. The effect is more pronounced in the case of PC when compared to PMMA (see *Figure 5b*). This increase of scattering will be referred to as 'excess', with respect to the non-deformed state. The excess appears to be maximum for $\beta = 0°$, i.e., when the shear stress direction and the incident light polarization are parallel. For $\beta = -55°$, this excess disappears so that deformed and non-deformed sample reduced spectra are identical up to $80\,cm^{-1}$ (*Figure 6a*). This anisotropy effect is clearly seen in *Figure 6b* where the reduced intensity of the non-deformed sample was subtracted from that of the sheared sample, for two β angle values, 0° and −55°.

The corresponding depolarized spectra also exhibit significant changes after a plastic shear. But it should be stressed here that two effects are superimposed in

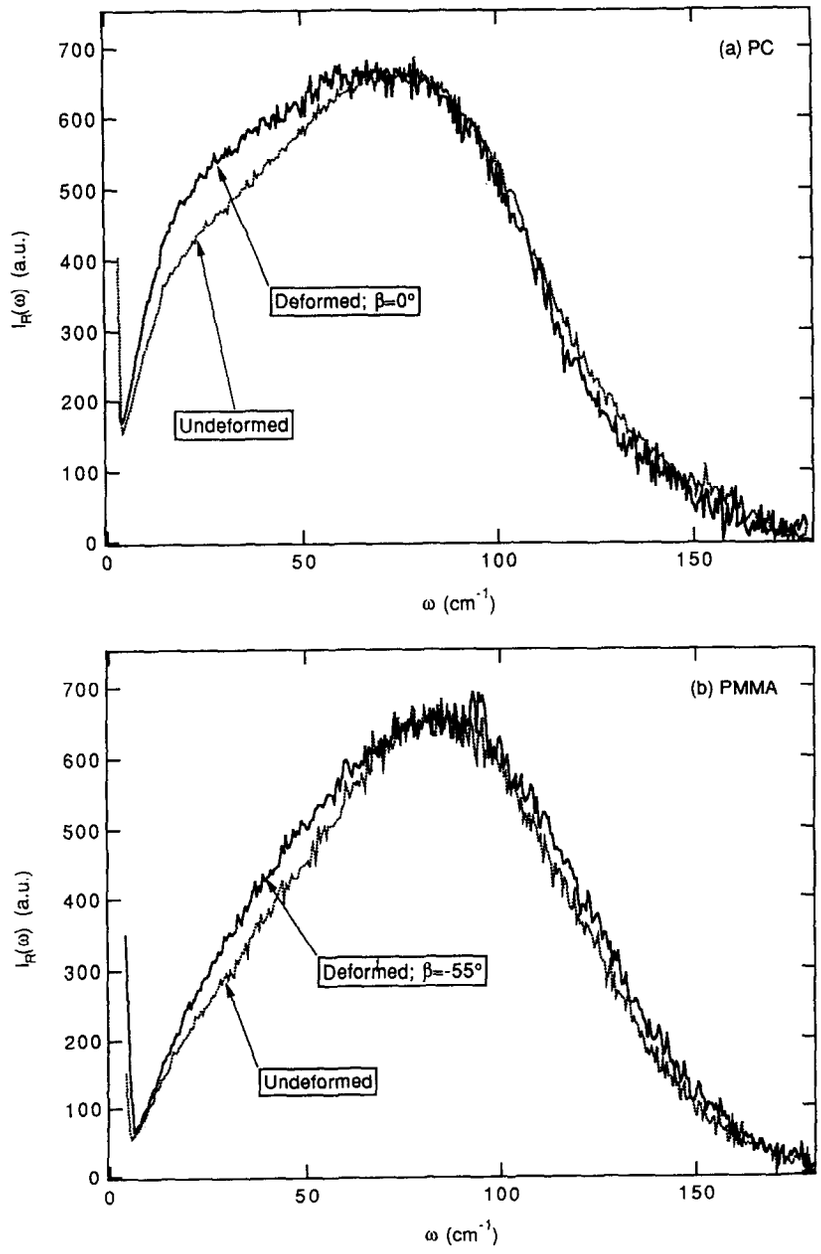


**Figure 5** LFRS reduced intensities $I_R(\omega)$ of (a) deformed (for $\beta - 0°$) and undeformed PC and (b) deformed (for $\beta = -55°$) and undeformed PMMA

these spectra: (1) the depolarization of the scattered light coming from the transversal or torsional vibrational modes, (2) the anisotropy resulting from the shear deformation. Because it is difficult to separate one from the other, interpretation of the observed effects is out of the scope of this paper, hence they will not be discussed here.

Besides the strong anistotropy and although the deformation appeared homogeneous on a macroscopic level for $\gamma = 1$, the LFRS showed some fluctuations around the mean curve displayed in *Figure 5a*, in the case of planar-concave calibrated parts: according to the location of the laser probed part along the $x$-axis, the intensity of the low-frequency excess, induced by plastic deformation, varies from strong to weak. Moreover, the excess progressively vanishes on probing regions that are further and further from the central $x$-axis.

The LFRS of the specimens which were deformed around $T_g$ presents similar features to those deformed at room temperature (*Figure 7*): again, $\beta = 0°$ appears to be a maximum excess orientation configuration (in VV conditions) and $\beta = -55°$ a minimum one. More interestingly, one can see a frequency shift of the broad band: it is a high-frequency shift for $\beta = -55°$ and a low-frequency shift (together with a great excess) for $\beta = 0°$.

*Cycled samples*

As seen from *Figure 8*, a similar excess as that observed with the deformed samples appears in the same frequency region, for identical polarization conditions (VV). However, if $\beta = 0°$ is still the orientation which corresponds to the largest excess, $\beta = -55°$ yields a comparatively smaller excess. Compared to the simply deformed samples, for which the excess completely vanishes for $\beta = -55°$, the cycled samples appear less anisotropic.

*Cycled and redeformed samples*

Like the previous samples, a comparable large LFRS excess is observed in polarized spectra (*Figure 9*). Similarly to the deformed samples, this excess is maximum for $\beta = 0°$ and nil for $\beta = -55°$. Here, the excess fluctuations along the central region of the sheared part are weaker than in the simply deformed samples. This homogeneity was confirmed by a much longer persistence of the excess from the centre to the sides of the deformed part.

## DISCUSSION

At first, apart from the nanoscopic structure which will

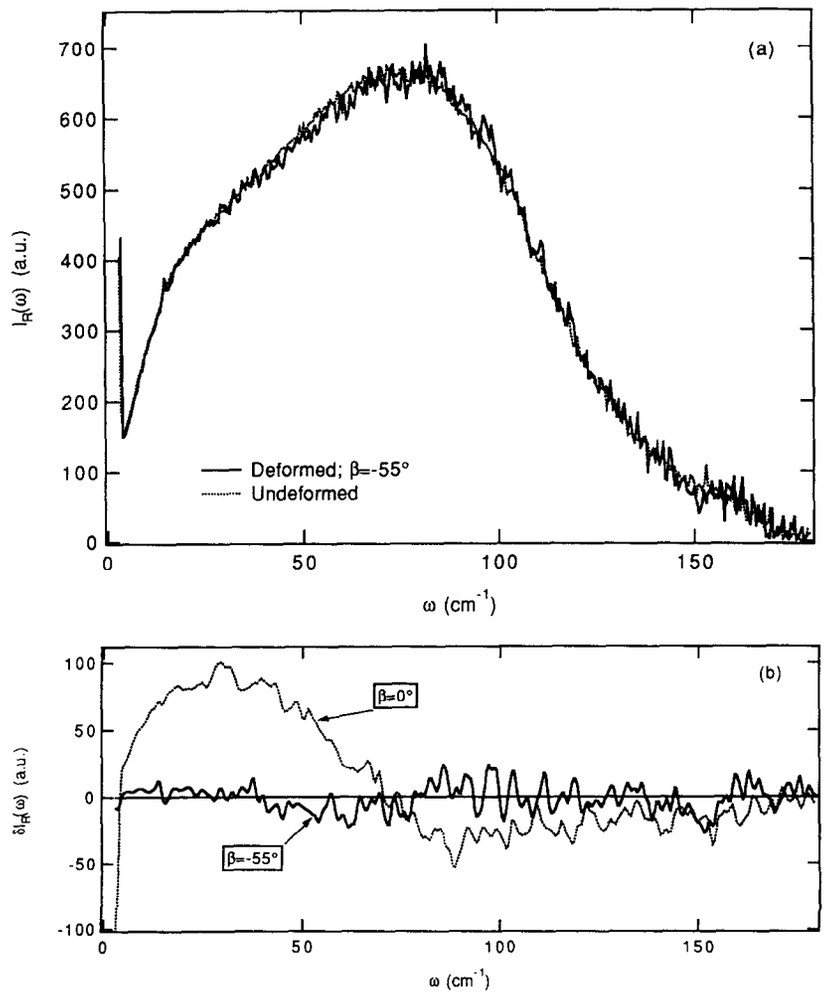


**Figure 6** (a) LFRS reduced intensities $I_R(\omega)$ of deformed (for $\beta = -55°$) and undeformed PC. (b) Difference LFRS reduced intensities $I_R(\omega)$ of deformed PC for $\beta = 0°$ and $\beta = -55°$ after subtraction of that of undeformed PC

be discussed in this section, from a macroscopic point of view both deformed and cycled samples appeared inhomogeneous towards the deformation effect. In a first approximation, this inhomogeneity scales with the laser spot size ($\emptyset \sim 100\,\mu m$). Since the same kind of measurements carried out with planar calibrated part specimens do not exhibit such a characteristic, the observed inhomogeneity is ascribed to the curvature of the calibrated part. In these latter type of samples, the thickness of the deformed part being smaller at the centre than over the sides, the deformation there can reach higher levels and then give rise to highly deformed zones.

The main feature which distinguishes plastically deformed samples from undeformed samples is, as reported above, a large and anisotropic light scattering excess that extends over the 4–80 $cm^{-1}$ spectral range, with a maximum at a wavenumber close to 35 $cm^{-1}$, which is larger than that of the boson peak. From the inverse proportionality of the wave number to the size of the vibrating unit[10], it is deduced that the vibrations which are responsible for the deformation induced anisotropic light scattering excess are localized over distances that are smaller than that of the cohesive regions which account for the existence of the boson peak. In addition, the position of the boson peak remains unchanged after deformation as can be observed in *Figure 6a* for $\beta = -55°$. From these remarks, it is deduced that the more cohesive regions are not or very little modified by the plastic deformation.

In these conditions, it is simply concluded that the deformation at the nanometric scale takes place in the less cohesive zones between the more cohesive regions. The low-energy anisotropic light scattering excess is due to an orientation of macromolecular strands that develop locally. Considering the assumed uneven cohesive nature

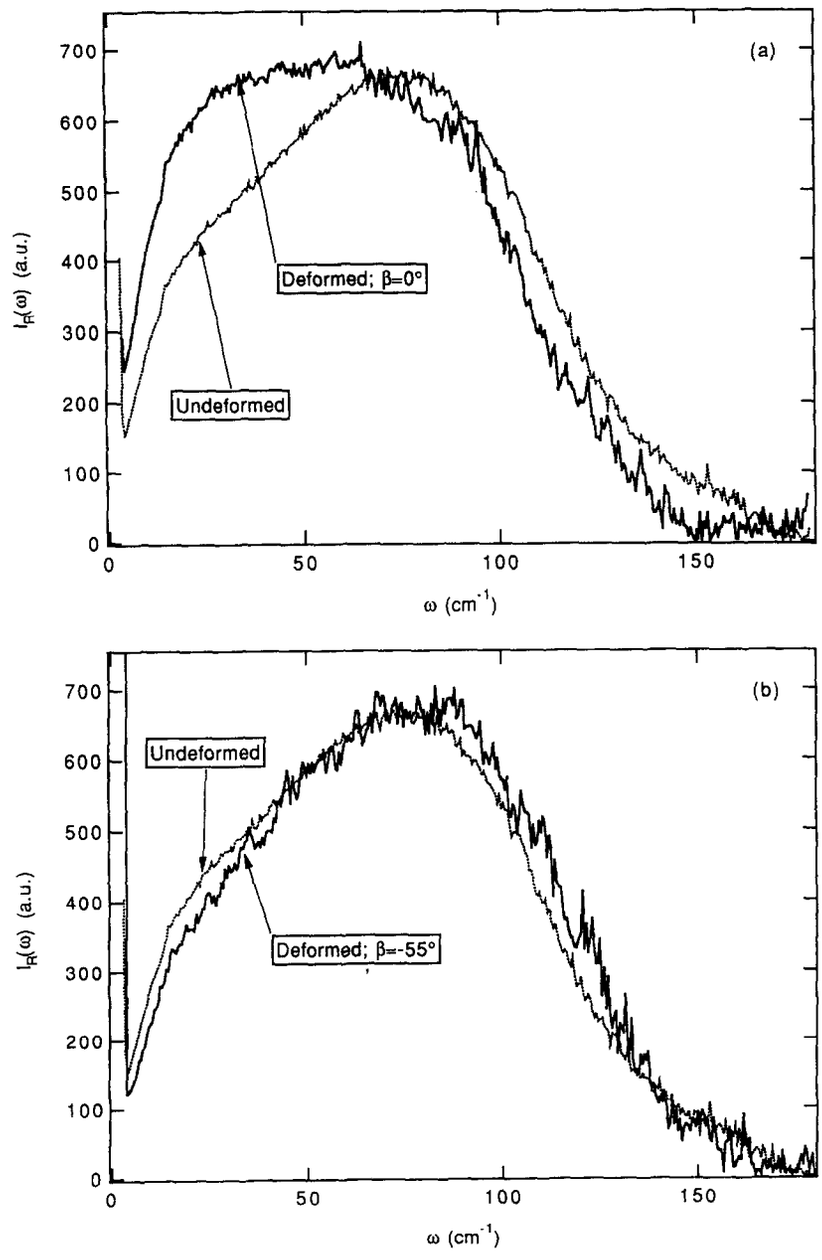


**Figure 7** LFRS reduced intensities $I_R(\omega)$of (a) PC deformed at $T \sim T_g$ (form $\beta = 0°$) and undeformed PC and (b) PC deformed at $T \sim T_g$ (for $\beta = -55°$) and undeformed PC

of the amorphous structure, it is not surprising that the molecular alignments develop in the weakly bonded regions.

Within such a picture frame, we shall now focus on what causes the excess to be maximum for $\beta = 0°$ and nil for $\beta = -55°$. The presence of aromatic rings in a PC monomer unit suggests a great sensitivity to polarization conditions. Polarizability is greatest in the plane of the aromatic cycles. Thus, if we consider that in the microscopically deformed regions of the sample, statistically most benzene rings are aligned in a plane, then there would exist a direction, perpendicular to this plane, for which the polarizability is the lowest[14]. Although the Raman signal originates in the vibration induced polarizability fluctuations and not in the polarizability itself, these two quantities are expected to be correlated. Consequently, $\beta = -55°$ corresponds to a configuration where the incident light polarization direction is orthogonal to the alignment plane, which is then inclined at $-55 + 90 = 35°$ with respect to the shear stress direction.

When considering the cycled samples, we observe that most deformation characteristics are reproduced except that the anisotropy is less marked. Therefore, the cycling strain procedure leading to a macroscopic state $\gamma = 0$, $\tau = 0$ does not significantly erase the effect of the first deformation at the nanoscopic scale: while the partial alignment of macromolecular strands in the less cohesive spaces remains, the orientation direction is less thoroughly respected from one interdomain to the other.

By carrying the same kind of deformation around $T_g$ instead of at room temperature, an additional observation was made: the broad band is more significantly shifted towards the high frequencies for $\beta = -55°$, compared to the undeformed state. As the broad band is the image of the material as a whole (it reflects all the acoustic vibrational states which are localized by the disorder), the observed shift reveals a modification of

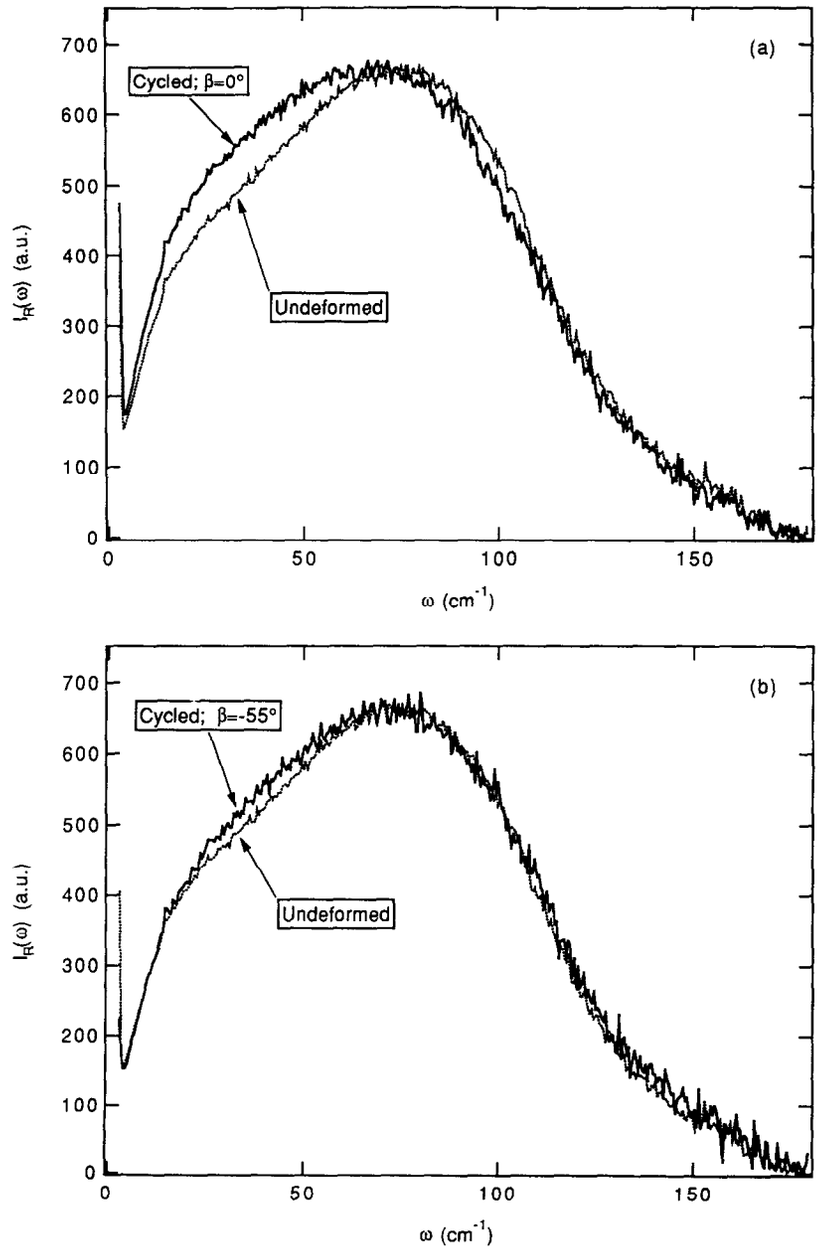


**Figure 8** LFRS reduced intensities $I_R(\omega)$of (a) cycled (for $\beta = 0°$) and undeformed PC and (b) cycled (for $\beta = -55°$) and undeformed PC

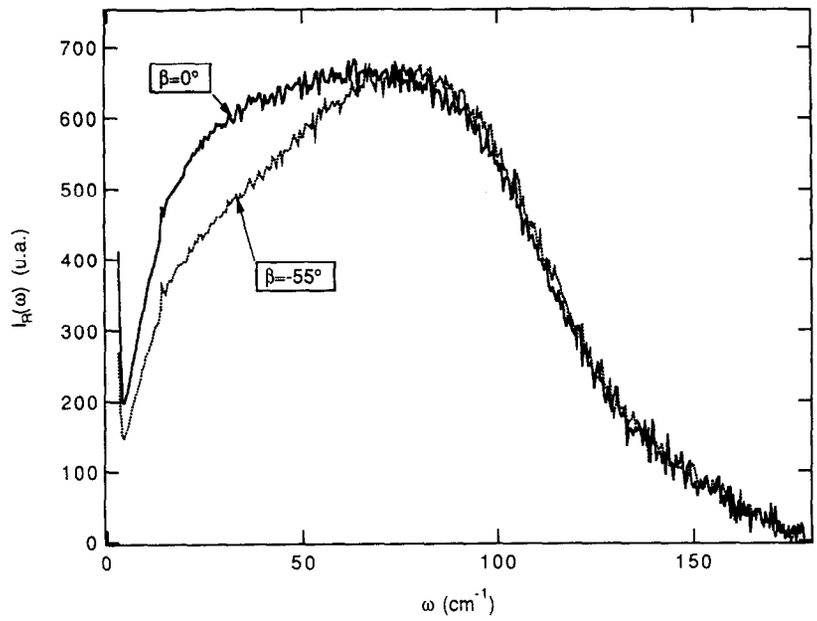


**Figure 9** LFRS reduced intensities $I_R(\omega)$ of redeformed PC for $\beta = 0°$ and $\beta = -55°$

the more cohesive regions which quantitatively make up the frame of the material. It means that both a partial orientation of the macromolecular strands in the more weakly bonded zones and a global deformation of the more cohesive regions occur in the deformation process. While the former modification induces an anisotropic low-energy excess, the latter modification gives rise to an anisotropic broad band shift. A very simple illustration of this consists of viewing the highly cohesive regions going from a pseudospheroidal shape to an ellipsoidal shape under the influence of the shear stress. In comparison with PC deformed at room temperature, the deformation is less localized. This is understandable since at the glass transition temperature the macromolecular chains start to become mobile, even in the more cohesive regions. Due to the thermal energy which then balances the intermolecular binding energy, the more cohesive regions can undergo plastic deformation at temperatures higher than $T_g$.

## CONCLUSION

The low-frequency Raman scattering of plastically deformed PC samples induced by a shear stress confirms the experimental results already obtained with PMMA[11]. The anisotropic low-frequency Raman scattering excess induced by a plastic deformation is much larger for PC than for PMMA. However, while in the case of PMMA the observed excess is maximum when both polarizations of the laser and the scattered light are perpendicular to the molecular orientation axis, it is minimum in the case of PC with these same polarization conditions. This difference is ascribed to the different dynamic polarizability tensors of PMMA and PC[14].

The deformation induced LFRS excess is interpreted as coming from oriented macromolecular strands in the less cohesive spaces between the more cohesive regions whose sizes are close to 4 nm. These cohesive regions are not or very little affected by a plastic deformation carried out at room temperature. However, as revealed by an anisotropic shift of the whole LFRS broad band in PC plastically deformed around $T_g$, the cohesive regions are deformed, due to the increase of the macromolecular chain mobility.

Two images of the non-continuous nanometric structure of the glassy polymers can be proposed: (1) the less cohesive spaces percolate through the material and the more cohesive regions or domains are isolated, (2) the more cohesive domains percolate and the less cohesive volumes are isolated. This second image is in agreement with the model of defects[15,16], where the assumed defects can be assimilated to the less cohesive domains. However, the first image, where the less cohesive spaces percolate, seems to be supported by the present results. Although the more cohesive and compact regions are non-crystalline, the arrangement inside these is expected to be greater than inside the less cohesive zones. In other words, an analogy can be made between nanocrystals and more cohesive regions on the one hand, and between amorphous phase and less cohesive zones on the other. Such analogy originates in the solidification process: after nucleation in different points of the material, the development of the more cohesive regions is stopped by the freezing of the surroundings before the bonding network in these surroundings can get stronger. Obviously this problem which has to do with the glass transition, deserves future study.

## REFERENCES

1 Shuker, R. and Gammon, R. W. *Phys. Rev. Lett.* 1970, **25**, 222
2 Martin, A. J. and Brenig, W. *Phys. Stat. Sol.* 1974, **64**, 163
3 Jäckle, J. 'Amorphous Solids', Springer-Verlag, Berlin, 1981, Chapter 8
4 Zemlyanov, M. G., Malinovsky, V. K., Novikov, V. N., Parshin, P. P. and Sokolov, A. P. *Pis'ma Zh. Eksp. Teor. Fiz.* 1990, **51**, 314; *JETP Lett.*, 1990, **51**, 359
5 Achibat, T., Boukenter, A. and Duval, E. *J. Chem. Phys.* 1993, **99**, 2046

6 Sokolov, A. P., Kisliuk, A., Quitmann, D. and Duval, E. *Phys. Rev.* B. 1993, **48**, 7692
7 Ahmad, N., Hussain, T. and Adkins, C. J. *J. Phys. Condensed Matter* 1993, **5**, 147
8 Duval, E., Boukenter, A. and Achibat, T. *J. Phys. Condensed Matter* 1990, **2**, 10277
9 Sokolov, A. P., Kisliuk, A., Soltwisch, M. and Quitmann, D. *Phys. Rev. Lett.*, 1992, **69**, 1540
10 Achibat, T. Boukenter, A. and Duval, E., Lorentz, G. and Etienne, S. *J. Chem. Phys.* 1991, **95**, 2949
11 Achibat, T. Boukenter, A., Duval, E., Mermet, A., Aboulfaraj, M., Etienne, S. and G'Sell, C. *Polymer* 1994, **36**, 251
12 G'Sell, C., Boni, S. and Shrivastava, S. *J. Mater. Sci.* 1983, **18**, 903
13 G'Sell, C. and Gopez, A. J. *J. Mater. Sci.* 1985, **20**, 3462
14 Munk, P. in 'Introduction to Macromolecular Science', John Wiley & Sons, New York, 1989
15 Mangion, M. B. M., Cavaillé, J. Y and Perez, J. *Philos. Magn.* 1992, **A66**, 773
16 Etienne, S. *J. Physique IV* 1992, **2**, C2-41